Computing vibrational energy relaxation for high-frequency modes in condensed environments

Dorita Rostkier-Edelstein, Peter Graf, and Abraham Nitzan
School of Chemistry, the Beverly and Raymond Sackler Faculty of Sciences, Tel Aviv University, Tel Aviv 69978, Israel

(Received 14 July 1997; accepted 27 August 1997)

In this paper we consider vibrational relaxation of high-frequency impurity modes in condensed environments as a computational problem. Linear response theory provides convenient routes for this computation: The vibrational relaxation rate is obtained as a Fourier transform of a force–force time correlation function. However, numerical difficulties arise for processes characterized by a direct relaxation of high-frequency modes into an environment characterized by a relatively low cutoff frequency. It is shown that modern signal processing procedures can significantly enhance the efficiency and accuracy of the needed computation. Since the relevant ''signal'' can be very small, the computation can be very sensitive to boundary conditions, and care must be taken to avoid artifacts. The computation may be facilitated by using the expected functional form, exponential dependence on the impurity frequency for high frequency, and fitting the parameters of this form from the simulation. It is emphasized that this exponential dependence seems to be the correct functional form, in spite of theoretical arguments in favor of a Gaussian dependence. The main difficulty in the numerical evaluation of the relaxation rate of high-frequency modes results from the fact that at low temperature the dynamical behavior of such modes is essentially quantum mechanical. We demonstrate this issue by considering vibrational relaxation of an impurity CO molecule in a low-temperature Ar matrix. The results obtained for this system by estimating the quantum correction to the classical force–force correlation function are consistent with experimental results, which indicate that under these conditions the relaxation of the vibrationally excited CO is dominated by radiative decay. © *1997 American Institute of Physics.* [S0021-9606(97)51445-0]

I. INTRODUCTION

Theoretical work on vibrational relaxation (VR) of solute molecules in condensed phases is still a focus of theoretical and experimental interest even after over 20 years of intensive research. It is safe to say that the main factors affecting this process in solid and liquid environments are now well understood. Among the important issues discussed and understood over the years are: (a) The interplay between the oscillator frequency and the spectrum of the thermal environment; (b) the effect of different types of solute–solvent interactions, in particular short range versus long range interactions; (c) the roles of different modes of motion: intramolecular modes of solute and solvent, local translational, librational, and rotational modes, and the solvent phonons, in the relaxation process; (d) temperature effects, and (e) the significance of the quantum mechanical aspects of the motion in the relaxation dynamics.

Within linear response theory, the vibrational energy relaxation rate, k_{VR}, of a harmonic bond in a thermal environment is given by (for a mode with frequency ω_0)[1–6]

$$k_{VR}=(2\mu)^{-1}\zeta(\omega_0), \tag{1}$$

where μ is the oscillator mass, $\zeta(\omega)$ is the frequency dependent friction defined by

$$\zeta(\omega)=(k_BT)^{-1}\int_{-\infty}^{\infty}dt\ \cos(\omega t)\langle F(0)F(t)\rangle, \tag{2}$$

k_B and T are the Boltzmann constant and the temperature, respectively, and F is the fluctuating solvent force ($\langle F\rangle=0$) on the oscillator coordinate. In evaluating Eq. (2) from molecular dynamics (MD) simulations, the oscillator bond is held rigid. Equations (1) and (2) are written for the classical limit. Quantum corrections to this results have been analyzed by Bader and Berne,[7] who have pointed out that for a harmonic Hamiltonian (harmonic oscillator interacting with a harmonic bath with bilinear interaction terms), Eqs. (1) and (2), with the correlation function in (2) evaluated from the classical trajectory, give also the correct quantum mechanical rate. It should be emphasized that this result is valid only for the particular model of linear coupling to a harmonic bath, and therefore is not appropriate for the relaxation of high-frequency modes, which requires nonlinear coupling to the bath. In general, the energy relaxation rate of a harmonic oscillator coupled to a general thermal bath with the interaction potential $V_{qb}=-qF$ (where q is the oscillator coordinate and F, the fluctuating force exerted by the bath on the oscillator, depends on the bath coordinates only) is given by ($\beta=(k_BT)^{-1}$),

$$k_{VR}=\frac{\tanh(\beta\hbar\omega/2)}{\beta\hbar\omega/2}\,\frac{\zeta_{QM}(\omega)}{2\mu}, \tag{3}$$

and the thermal transition rate between two levels in a system coupled to its environment via the interaction potential $H_{sb}=-S(q)F$ (S is a system operator) is

Downloaded 21 Mar 2004 to 132.66.16.12. Redistribution subject to AIP license or copyright, see http://jcp.aip.org/jcp/copyright.jsp

$$k_{I\to J}=\frac{2|S_{IJ}|^2}{\beta\hbar^2[1+\exp(-\beta\hbar\omega_{IJ})]}\,\zeta_{QM}(\omega_{IJ})$$
$$=e^{\beta\hbar\omega_{IJ}}k_{J\to I}, \tag{4}$$

where[7]

$$\zeta_{QM}(\omega)=\beta\int_{-\infty}^{\infty}dt e^{i\omega t}\left\langle\frac{1}{2}[F(t),F(0)]_+\right\rangle$$
$$=\beta\int_0^{\infty}dt\,\cos(\omega t)\langle[F(t),F(0)]_-\rangle. \tag{5}$$

It is possible to use Eqs. (3)–(5) as a starting point for evaluating quantum corrections factors to rates evaluated from the classical ''force''–''force'' correlation function in more general cases, e.g., with nonlinear coupling. For our discussion here it is sufficient to note that, as in many other situations, Fourier transforms of time correlation functions play a central role in both classical and quantum rate theories.

Numerical simulations aimed at evaluating vibrational relaxation rates of solute molecules using Eqs. (1) and (2) [or Eqs. (3) with $\zeta_{QM}(\omega)$ replaced by its classical counterpart, Eq. (2)] have been recently used by several workers.[3–5,8–12] Within given uncertainties in the interaction potentials and with possible correlation resulting from the quantum nature of the thermal environment,[7] these calculations may be considered to be moderately successful. A very important attribute in calculations based on Eqs. (1)–(5) lies in the fact that relatively short time correlation functions are used to calculate relatively slow rates. Still, when the VR process can be viewed as a high-order multiphonon transition, i.e., when there is a large mismatch between the relaxing mode frequency and the frequencies of the accepting modes (e.g., a high-frequency diatomic molecule solute in a low Debye frequency atomic solvent[13]), even this approach may be very difficult because the Fourier transform in Eqs. (2) or (5) must be carried out with frequency much larger than the inverse characteristic times associated with the friction kernel, which yields a very small rate subjected to very large numerical errors. As a mathematical issue, evaluating the rate becomes a signal processing problem. From the physical point of view, the nature of the interaction and the relevant motions responsible for this high-frequency part of the response are essential.

As a numerical problem, evaluating the high-frequency Fourier components of correlation functions like those appearing in Eqs. (2) or (5) is hampered by the fact that the Fourier transform $\zeta(\omega)$ falls to zero very rapidly for $\omega>\omega_D$ (ω_D being the ''Debye frequency'' of the solvent). Thus, we need to evaluate a very small signal in the presence of very large noise. It may help to have some notion about the way $\zeta(\omega)$ depends on ω. Some confusion arises from the common intuitive association of high frequencies with short times. Adelman and co-workers,[6] in fact, suggest that the relaxation rate of high-frequency diatomic solutes in simple fluid is necessarily a Gaussian dependence on the frequency, $k_{VR}\sim\exp(-a\omega^2)$, since the initial relaxation of time correlation functions is quadratic, $C(t)\sim 1-bt^2\cong\exp(-bt^2)$. Similar conclusions may be reached from approaches based on instantaneous normal modes (INM),[14] if one makes the seemingly reasonable assumption that relaxation of high-frequency impurity modes is dominated by short time motions in the environment that can be analyzed within the INM picture. However, while the short time quadratic time dependence of the correlation function is implied by symmetry considerations, it *does not* imply a Gaussian high-frequency dependence in Fourier space. This has been known in the VR literature for some time,[5,9] and a non-Gaussian behavior—the exponential ''energy gap law'' has already been suggested a long time ago.[15] However, since the high-frequency Gaussian behavior of spectral line shapes is a deeply rooted notion, it is useful to examine this issue more closely. To this end we consider the Kubo function,

$$C(t)=\exp\left[-\alpha^2\left(\frac{t}{\alpha}-+e^{-t/\alpha}\right)\right], \tag{6}$$

as a simple example. This function is well known in the stochastic theory of line shapes[16] as a precursor of the absorption line shape, $J(\omega)$, of an oscillating dipole whose frequency has a stochastic white-noise component. $J(\omega)$ is given by the Fourier transform

$$J(\omega)=2\int_0^{\infty}dt\,\cos(\omega t)C(t). \tag{7}$$

Kubo's theory[16] predicts a Lorentzian line shape, $(\omega^2+\alpha^2)^{-1}$, near the absorption center and a Gaussian, $\exp(-\omega^2/2)$, in the band edges.[17] However, we show in the Appendix that the truly asymptotic ($\omega\to\infty$) form of (7) is not a Gaussian but a power law, ω^{-4}. The Kubo function provides a successful model for the transition from the Lorentzian center to the Gaussian edges of absorption line shapes in condensed environments because the truly asymptotic regime $\omega\to\infty$ is irrelevant in such applications. The situation is very different in the case of vibrational relaxation of high-frequency solutes imbedded in low-frequency condensed environments. As we show below, numerical simulations seem to confirm the theoretical prediction[15] that at least in the relevant experimental range, the exponential energy gap law, $\zeta(\omega)\sim\exp(-\alpha\omega/\omega_D)$, where α is a constant and ω_D is a measure of the extent of the solvent intermolecular spectrum—the equivalent of the Debye frequency in solids, holds.

II. PHYSICAL MODELS AND SIMULATION DATA

In the examples shown and discussed below, we consider the vibrational relaxation of a diatomic molecule solvated in either a Lennard-Jones (LJ) or a Stockmayer fluid. The first is characterized by the intermolecular potential

$$V_{\rm LJ}(r)=-4\varepsilon_{\rm LJ}\left[\left(\frac{\sigma_{\rm LJ}}{r}\right)^6-\left(\frac{\sigma_{\rm LJ}}{r}\right)^{12}\right], \tag{8}$$

and in the second this potential is supplemented by putting a point dipole μ at the center of each LJ sphere, i.e., the interaction between two solvent particles i and j is

Downloaded 21 Mar 2004 to 132.66.16.12. Redistribution subject to AIP license or copyright, see http://jcp.aip.org/jcp/copyright.jsp

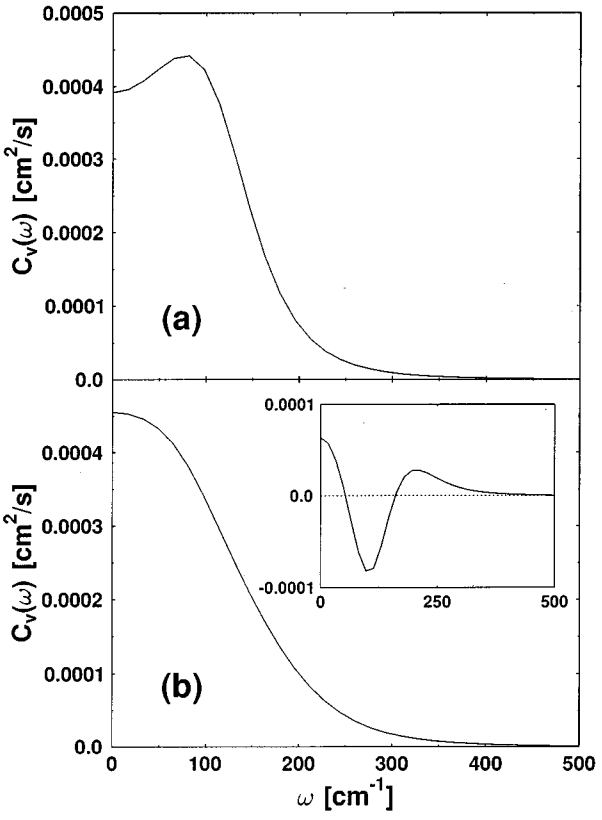

FIG. 1. Fourier transforms of the velocity–velocity time correlation functions, $C_v(\omega)=2\int_0^\infty dt\ \cos(\omega t)\langle \mathbf{v}(0)\cdot\mathbf{v}(t)\rangle$, for (a) the ''standard'' LJ model, and (b) the ''standard'' Stockmayer model. The inset in Fig. 1(b) shows the difference between the two.

$$V(\mathbf{r}_{ij})=V_{\mathrm{LJ}}(r_{ij})+\frac{\boldsymbol{\mu}_i\cdot\boldsymbol{\mu}_j-3(\hat{n}\cdot\boldsymbol{\mu}_i)(\hat{n}\cdot\boldsymbol{\mu}_j)}{r_{ij}^3}. \tag{9}$$

In what follows, we refer by ''standard model'' to the following choice of parameters: $\sigma_{\mathrm{LJ}}=3.15$Å, $\varepsilon_{\mathrm{LJ}}=78.3$ K, the mass $M=18$ amu, the moment of inertia $I=1.284$ amu·Å^2, the temperature $T=298$ K, and the density $\rho=1.0$ g/cm^3. These are parameters that were used to fit water molecules within the Stockmayer model.[18,19] The dielectric moment of this waterlike Stockmayer fluid was taken to be 1.695 D. With this choice, the dielectric constant calculated as described in Ref. 20 was found to be $\varepsilon\sim 80$. The Fourier transforms of the velocity–velocity time correlation functions of this Stockmayer liquid and of the corresponding LJ liquid characterized by the same parameters, except that $\mu=0$, are shown in Fig. 1. These spectra reflect the contributions of translational motions for the LJ fluid and of translational and rotational motions for the Stockmayer system. The difference spectrum [inset in Fig. 1(b)] emphasizes the contribution of rotational and librational degrees of freedom for $\omega\geqslant 150$ cm^{-1}. Our solute is a generic dipolar diatomic molecule, which for definiteness is taken identical to the diatomic CH_3CL model considered in Ref. 4. The atomic masses in this model are those of CH_3 and of Cl. These ''atoms'' interact with the solvent with a combination of LJ interactions and Coulombic interactions associated with the partial charges $q_{\mathrm{CH3}}=-q_{\mathrm{Cl}}=0.25$ e. The LJ parameters for the solute–solvent interactions are obtained by taking $\sigma_{\mathrm{Cl}}=3.93$ Å, $\sigma_{\mathrm{CH3}}=3.43$ Å, $\varepsilon_{\mathrm{Cl}}=90.68$ K, and $\varepsilon_{\mathrm{CH3}}=53.63$ K and using the combination rules $\sigma_{ij}=[\sigma_i+\sigma_j]/2$ and $\varepsilon_{ij}=(\varepsilon_i\varepsilon_j)^{1/2}$. The solute equilibrium bond length is $R_{\mathrm{eq}}=1.78$ Å, and the intramolecular interaction is a Morse potential characterized by a well depth $D_0=234.52$ Kcal/mol and a bottom frequency $\omega=680$ cm^{-1}. Note, however, that in the simulation this bond is held rigid.

In Sec. V below we also apply our numerical consideration to one realistic system: an impurity CO molecule imbedded in an argon matrix. The model for this system assumes Lennard-Jones interactions between the argon atoms as well as between them and the carbon and oxygen atoms. The parameters used are[21,22] σ(Ar–Ar)=3.42 Å, σ(Ar–O)$=\sigma$(Ar–C)=3.28 Å, ε(Ar–Ar)=124 K, ε(Ar–C)$=\varepsilon$(Ar–O)$=$88 K. The CO bond length is 1.1 Å and is frozen during the simulation. In all simulations we use 399 Ar atoms and 1 CO molecule in a cubic box of length 25.136 Å, which corresponds approximately to the density of Ar in a 20 K matrix. (Note that the same density was used for simulations made at higher temperatures.) The simulated system was prepared by first equilibrating it at room temperature, then quenching it to the desired low temperature. The resulting system is therefore amorphous and the calculated rate will depend somewhat on the particular local configuration surrounding the CO molecule.

Below we compute the resulting relaxation rate as a function of several of these parameters, primarily ω. The simulated system consists of 100–400 solvent particles and 1 solute molecule in a cubic cell of size $L=14.364$ Å (100 particles; twice that for 400 particles). In typical trajectories we used 40 000–100 000 time steps with $\Delta t=1$ fs after the system was equilibrated. The dynamics of the Stockmayer fluid is obtained using the SHAKE algorithm as described in Ref. 23. As we see below, the quality of the computed rate may be sensitive to the way boundary conditions are handled. In order to examine this issue we have used different cutoff schemes for both the LJ and for the electrostatic interactions. For the LJ potential the following two cutoff schemes were used:

$$V_{\mathrm{LJ}}^A(r)=V_{\mathrm{LJ}}(r)\,\theta(R_c-r), \tag{10}$$

$$V_{\mathrm{LJ}}^B(r)=\left\{V_{\mathrm{LJ}}(r)-V_{\mathrm{LJ}}(R_c)-48\varepsilon_{\mathrm{LJ}}\left[\frac{1}{2}\left(\frac{\sigma_{\mathrm{LJ}}}{R_c}\right)^6-\left(\frac{\sigma_{\mathrm{LJ}}}{R_c}\right)^{12}\right]\frac{r-R_c}{R_c}\right\}\theta(R_c-r), \tag{11}$$

where $\theta(x)=1$ for $x>0$ and is zero otherwise. The second choice keeps the force (first derivative of the potential) continuous at the cutoff radius, while the first choice does not.

For the electrostatic interactions we use either reaction field (RF) boundary conditions (see Ref. 23 for details) or periodic boundary conditions with Ewald sums (ES) in order to treat the long range electrostatic interactions. In the RF case, electrostatic interactions are cut off at the reaction field radius $R_c=L/2$. This cutoff is affected by a function that

Downloaded 21 Mar 2004 to 132.66.16.12. Redistribution subject to AIP license or copyright, see http://jcp.aip.org/jcp/copyright.jsp

goes to zero between $R_s = fR_c$ and R_c (we took $f = 0.95$). The simplest (and most commonly used) cutoff form is

$$V_{DD}^{A}(\mathbf{r}_{ij}, \boldsymbol{\mu}_i, \boldsymbol{\mu}_j) = \left\{ \left(\frac{1}{r_{ij}^3} - \frac{2(\varepsilon' - 1)}{(2\varepsilon' + 1) R_{\mathrm{eff}}^3} \right) \boldsymbol{\mu}_1 \cdot \boldsymbol{\mu}_j - \frac{3(\hat{n} \cdot \boldsymbol{\mu}_i)(\hat{n} \cdot \boldsymbol{\mu}_j)}{r_{ij}^3} \right\} t^A(r_{ij}) \times \theta(R_c - r_{ij}), \tag{12}$$

with the tapering function

$$t^A(r) = \begin{cases} 1 & r < R_s \\ 1 - \dfrac{r - R_S}{R_c - R_s}; & R_{\mathrm{eff}}^3 = (1 + f + f^2 + f^3) R_c^3/4 \, . \\ 0 & R_c < r \end{cases} \tag{13}$$

With this choice, the potential energy is continuous at the sphere boundary but the forces are not. A slightly modified form, V_{DD}^{B}, is similar to (14), with t^A replaced by

$$t^B(r) = \begin{cases} 1 & r < R_s \\ 1 - 3\left(\dfrac{r - R_S}{R_c - R_s} \right)^2 + 2\left(\dfrac{r - R_S}{r_c - R_S} \right)^3 & R_S < r < R_c, \\ 0 & R_c < r \end{cases} \tag{14}$$

and $R_{\mathrm{eff}}^3 = (1 + (3/2)f + (3/2)f^2 + f^3) R_c^3/5$, which renders both potential and force continuous at the boundary. In the Ewald approach, the electrostatic energy and forces are given as sums of terms, computed in real and reciprocal spaces. The real space sum is usually restricted to the first simulation cell and a parameter α determines both the error in this truncation and the corresponding number of terms that needed to be taken in the reciprocal space summation to achieve a similar truncation error. α has to be large enough so that limiting the sum in real space to the first simulation cell (i.e., to a cutoff distance $R_c \sim L/2$) is valid. Using this cutoff the truncation error is of the order $\delta = \exp(-\alpha^2/4)$.[24,25] We have checked the accuracy of the computed rate with respect to the choice of α or δ, as detailed below.

III. COMPUTING VIBRATIONAL RELAXATION RATES AS A SIGNAL DETECTION PROBLEM

As discussed in the Introduction, the use of Eqs. (2) or (5) to evaluate vibrational relaxation rates from numerical simulation data has a considerable advantage over the direct observation of energy relaxation as a function of time. To get meaningful results for the latter, one needs to follow the (relatively slow) relaxation process of interest, while the force–force correlation functions of Eqs. (2) and (5) relax on the much shorter time scale associated with the solvent nuclear motion. This important time-saving device should be used with care for frequencies much higher than those characteristic to the solvent: The friction $\zeta(\omega)$ goes to zero very quickly with ω in this range, so simply evaluating the Fourier transform in (2) or (5) amounts to detecting a very small signal in the presence of much stronger irrelevant ones. This problem is compounded by the fact that the correlation functions $\langle F(0)F(t) \rangle$ or $\langle [F(t), F(0)]_+ \rangle$ are not known exactly: They are obtained at a finite number of discrete time points and by necessity are affected by numerical inaccuracies and by statistical noise.

The issue outlined above is a standard problem in signal processing, and is discussed in a large body of available literature (see, e.g., Ref. 26; for an introductory review see Ref. 27). In view of the very demanding nature of our type of signal processing, it is worthwhile to consider ways and means offered by this literature. For the sake of definiteness we focus on the force–force time correlation function $\langle F(0)F(t) \rangle$ of Eq. (2). It is assumed that we have obtained the desired force as a (real valued) data sequence $F[n] = F(n\Delta t)$, where Δt is the chosen time interval and $n = 0,1,...,N-1$. The following points ca be of relevance:

(a) For a given sampling interval Δt, the Fourier transform is meaningful only for $|\omega| \leqslant \omega_c = \pi/(\Delta t)$. ω_c is the Nyquist critical frequency. When the sampling is restricted to the N points $t = n\Delta t$, $n = 0,1,...,N-1$, the discrete Fourier transform is defined by

$$\hat{F}_k \equiv \hat{F}(\omega_k) = \sum_{n=0}^{N-1} F[n] e^{-i\omega_k n \Delta t}; \qquad \omega_k = 2k/(N\Delta t) \quad \text{with} \quad k = -N/2,...,(N/2-1).$$

$\Delta t \hat{F}(\omega_k)$ is hopefully a decent approximation to $\int_{-\infty}^{\infty} dt F(t) e^{i\omega_k t}$. The correlation function is defined by

$$C[l] = \frac{1}{N} \sum_{n=0}^{N-|l|-1} F[n] F[n + |l|]. \tag{15}$$

(b) The discrete sampling defined above provides an exact representation for a function which is band limited to the interval $\omega < \omega_c$. The transform of functions which are not band limited to this range may suffer from aliasing: The power spectrum outside the Nyquist range is spuriously moved into that range. This is not expected to create a serious problem in our present application, because our spectrum decreases rapidly for $\omega > \omega_D$, where ω_D is the solvent ''Debye frequency,'' provided we chose the sampling such that $\omega_c > \omega_D$.

(c) The Wiener–Khinchin theorem, which relates the Fourier transform of the correlation function $\langle F(0)F(t) \rangle$ to the absolute square of the Fourier transform of $F(t)$ takes the following form for finite discrete samples: Let

$$\hat{C}(\omega) = \sum_{l=-(N-1)}^{N-1} C[l] e^{i\omega l \Delta t} \tag{16}$$

and

$$\hat{F}(\omega) = \sum_{n=0}^{N-1} F[n] e^{-i\omega n \Delta t}. \tag{17}$$

Then

$$\hat{C}(\omega) = \frac{1}{N} |\hat{F}(\omega)|^2. \tag{18}$$

Downloaded 21 Mar 2004 to 132.66.16.12. Redistribution subject to AIP license or copyright, see http://jcp.aip.org/jcp/copyright.jsp

This result is very useful for our application: It turns out that results based on (18) are more reliable in the high-frequency limit.

(d) Given that $F[n]$ is a random signal, the *periodogram* $\hat{C}(\omega)$ is another discrete random function. Its mean is obviously positive for all N, and approaches asymptotically $(N\to\infty)$ the *power density spectrum* of the process. However, *its variance remains finite, of the order of the square of its mean, in this limit*. The standard deviation of this estimate of the power spectrum is therefore of the same order as the mean, and extra effort is needed to increase accuracy. This can be done by either breaking the data set into smaller segments and averaging the periodograms associated with different segments, computing the periodogram with finer discrete frequency spacing than needed, then coarse-graining the resulting periodogram estimate by summing the values within bins of predefined size in the frequency domain, and/or using data windowing [see, e.g., Refs. 27 (Sect. 12.7) and 28].

(e) The power spectrum estimate given by the periodogram

$$\hat{F}(\omega_k)=\left|\sum_{n=-N/2}^{N/2-1} F[n]e^{-2\pi ikn/N}\right|^2; \quad \omega_k=2\pi k/(N\Delta t), \tag{19}$$

or

$$\hat{F}(z)=\left|\sum_{n=-N/2}^{N/2-1} F[n]z^n\right|^2; \quad z\equiv e^{-2\pi ik/N}, \tag{20}$$

is just one possible form for an approximate estimate to the true power spectrum. [A formal expression for representing the latter is similar to (20) with the sum extended to $-\infty\ldots\infty$, i.e., by an infinite Laurent series.] This is the ''all zero model,'' emphasizing the fact that the model spectrum can have zeros, but not poles in the complex z plane. A powerful alternative is the ''all pole model,'' based on the form

$$\hat{F}(z)\approx\frac{a_0}{\left|1+\sum_{k=1}^{M} a_k z^k\right|^2}. \tag{21}$$

In principle, the $M+1$ coefficients a_k may be determined so that the first $M+1$ terms in a power series expansion of (21) agree with the equivalent terms in the infinite Laurent series corresponding to (20). In practice, these coefficients are often obtained from the following set of linear equations (the ''maximum entropy method,'' MEM)

$$\begin{bmatrix} C_0 & C_1 & C_2 & \cdots & C_M \\ C_1 & C_0 & C_1 & \cdots & C_{M-1} \\ C_2 & C_1 & C_0 & \cdots & C_{M-2} \\ \cdots & & & & \cdots \\ C_M & C_{M-1} & C_{M-2} & \cdots & C_0 \end{bmatrix} \begin{bmatrix} 1 \\ a_1 \\ a_2 \\ \\ a_M \end{bmatrix} = \begin{bmatrix} a_0 \\ 0 \\ 0 \\ \cdots \\ 0 \end{bmatrix}, \tag{22}$$

where $C_{\ell}=C_{-\ell}$ is the correlation function (15) at time lag $\ell\Delta t$.

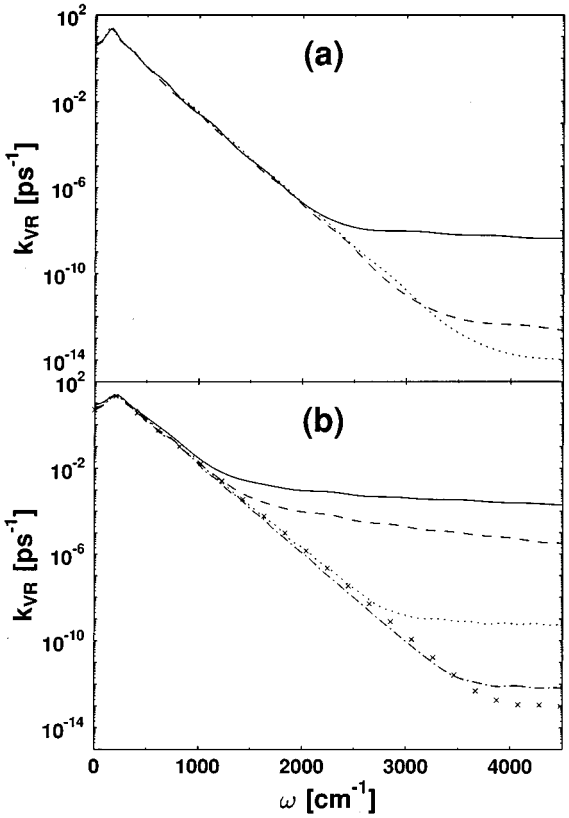

FIG. 2. The vibrational energy relaxation rate, Eq. (1) calculated for a mode with reduced mass $\mu=18$ amu for (a) the ''standard'' LJ fluid, and (b) the ''standard'' Stockmayer fluid. In (a) the full line results from a system of $N=128$ particles, with the interparticle potential given by V_{LJ}^{A} [Eq. (12)], with $R_c=L/2$ and the dashed and dotted lines corresponding to systems of $N=128$ ($L=15.62$ Å) and $N=256$ ($L=19.68$ Å) particles, respectively, with the potential V_{LJ}^{B} [Eq. (13)]. In (b), the full and dashed lines correspond to systems of $N=128$ ($L=15.62$ Å) with reaction field boundary conditions ($R_c=L/2$), using, respectively, V_{DD}^{A} [Eqs. (14) and (15)] and V_{DD}^{B} [Eq. (14) with t^A replaced by t^B, Eq. (16)]. In both cases, V_{LJ}^{A} was used for the LJ interactions; however, using V_{LJ}^{B} in these cases had no significant effect. The other three lines are obtained by using periodic boundary conditions with Ewald sums: For the dotted line $N=128$ and $\delta=10^{-4}$ for the dashed–dotted line, $N=128$ and $\delta=10^{-6}$, and for the crosses, $N=256$ and $\delta=10^{-6}$. In these three cases V_{LJ}^{B} was used for the LJ interaction. The maximum entropy method was used in all cases.

In addition to the ''standard'' issues outlined above, there are several other issues associated with our specific signal processing problem.

As already noted, many of our applications deal with the energy relaxation of a high-frequency mode of a solute molecule in a bath whose dynamics reflects a relatively low cutoff (Debye) frequency. A typical example is the vibrational relaxation of a diatomic molecule in rare gas solids. In this situation, our ''signal'' is extremely small and our computations may be extremely vulnerable to computational artifacts. An example of such artifacts is provided by the sensitivity of the computed friction, $\zeta(\omega)$, to the boundary conditions. This is demonstrated in Fig. 2, which shows the friction as a function of frequency for our ''standard'' LJ and Stockmayer

Downloaded 21 Mar 2004 to 132.66.16.12. Redistribution subject to AIP license or copyright, see http://jcp.aip.org/jcp/copyright.jsp

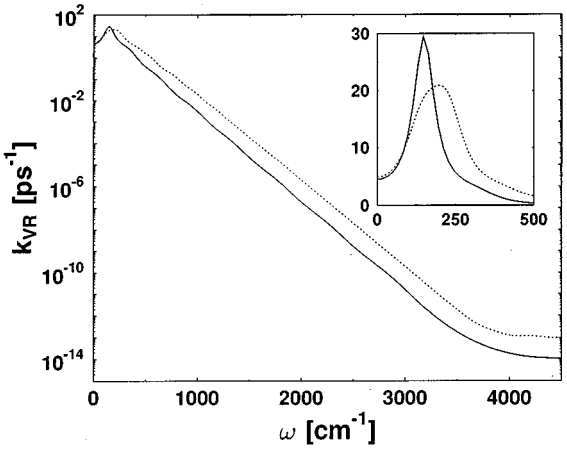

FIG. 3. The two best (lowest) lines from Figs. 2(a) and 2(b), respectively. Full line is the ''vibrational relaxation rate'' computed (see text) in the ''standard'' Stockmayer fluid. Dotted line—same as for the ''standard'' LJ fluid.

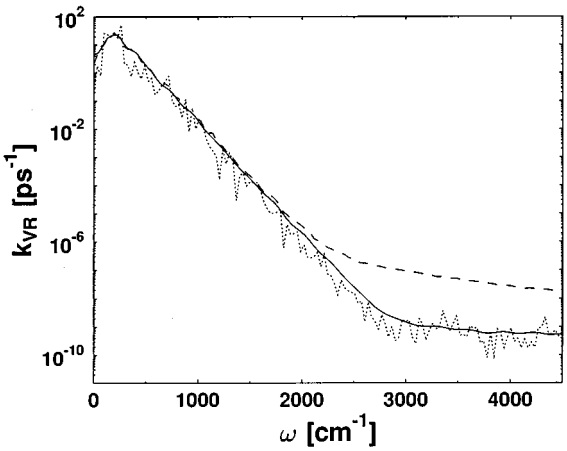

FIG. 4. A comparison of three different data analysis schemes using a data set corresponding to the force acting on one particle in the ''standard'' Stockmayer fluid in the dipole direction, sampled at intervals of 1 fs. Dashed and dotted lines are averages over periodograms calculated for segments of different lengths. The full lines are obtained from the maximum entropy method with 70 poles. See text for details.

solvents. In order to save computer effort we simplify this test calculation by using the pure solvents, and the ''friction'' is calculated from a force–force time correlation function, where the force is that exerted on any solvent molecule by all other molecules in the direction of its dipole (or in some fixed direction in the LJ system). Figure 2(a) shows the result for the LJ solvent ($\mu=0$), and Fig. 2(b) shows similar results for the Stockmayer fluid. A significant observation is that for large ω the computed friction is quite sensitive to the boundary conditions, in particular in the system with long range Coulombic interactions. Thus in the Stockmayer system, a crossover to an unphysically weak frequency dependence of the friction occurs at some high frequency whose magnitude depends on the boundary model used (reaction field or Ewald sum), and on the cutoff function imposed on the long range potential in the model that uses reaction field boundary conditions. The origin of this sensitivity is the fact that the very small response at high frequency may be affected by unphysical contributions to the force associated with particles that cross the interaction cutoff range. Such unphysical contributions are usually too small to affect most other properties, but may not be too small in the present context. Figure 2(b) shows that a careful choice of model, system size, and boundary conditions may significantly improve the reliability of the computed friction; however, calculational artifacts associated with the system boundary may contaminate the results if such precaution is not taken.

It is interesting to note in passing the effect of Coulombic interactions on the relaxation rates. Figure 3 compares the two best (lowest) lines from Figs. 2(a) and 2(b) which correspond to systems that differ from each other only by the existence of a permanent molecular dipole in the latter. The potentially important role of electrostatic interactions in affecting vibrational energy transfer to the solvent has been discussed by several workers.[3–5,8,29] It has been pointed out that the availability of rotational and librational modes in polar solvents can enhance vibrational relaxation of solute modes whose frequencies lie in the corresponding range (see, however, Ref. 12). This effect is also seen here at low frequencies (see inset to Fig. 3); however, multiphonon relaxation of high-frequency solute modes is seen to be dominated by the short range interactions. In fact, for the present model, the LJ fluid is seen to be more effective than the corresponding Stockmayer fluid in affecting the relaxation at high solute frequencies. The reason for this may be that the solvent structure about the solute is held tighter in the polar system, preventing the close encounters needed for multiphonon relaxation.

The calculation of a very weak high-frequency response as is required here may be subject to other computational artifacts. We have found that an important reliability test is provided by comparing results obtained using the ''all zeros'' (direct Fourier transform) and the ''all poles'' (maximum entropy) forms for the estimate of the spectral response. An agreement between computations based on these different approximations provides a strong indication for the integrity of the result. Figure 4 shows an example of such a comparison. The data set used to produce these results represents the force $F[n]$ sampled at 40 000 points along a trajectory obtained for the Stockmayer fluid with $\Delta t=1$ fs (periodic boundary conditions using Ewald sums with $\delta=10^{-4}$). The dashed line is obtained by first dividing the data set into overlapping segments of 1024 points each (neighboring segments overlap over half of their lengths), performing the Fourier transform on each segment using a triangular window, and averaging the absolute squares of the resulting transforms over all segments. The dotted line is obtained from the same procedure, using segment lengths of 8192. This gives an overall increase in accuracy at high ω; however, the fewer segments used imply larger noise. The full line is obtained from the maximum entropy method using 71 parameters (70 poles).

Knowledge of the asymptotic form of $\zeta(\omega)$ for $\omega\rightarrow\infty$ can

Downloaded 21 Mar 2004 to 132.66.16.12. Redistribution subject to AIP license or copyright, see http://jcp.aip.org/jcp/copyright.jsp

facilitate its evaluation in this regime. Arguments based on the saddle point approximation, as well as numerical evaluation of the Fourier transform of simulated force–force correlation functions, suggest an exponential ''energy gap law,'' $\zeta(\omega)=A\exp(-\alpha\omega)$, where A and α are positive constants. Assuming that this indeed is the correct asymptotic form, i.e., that the function $C(t)$ satisfies

$$\hat{C}(\omega)\equiv\int_{-\infty}^{\infty}dte^{i\omega t}C(t)\sim Ae^{-\omega/\omega_0};\quad \omega\rightarrow\infty, \tag{23}$$

our task reduces to calculating $A$and ω_0. Figures 2(a) and 2(b) show that we could extract the parameters for an exponential dependence of the rate from any of the lines displayed. Alternatively, the following procedure was found to be useful when $C(t)$ is the force–force correlation function: Since we look for the asymptotic behavior at large ω, it is reasonable to expect that it is dominated by the short time part of $C(t)$. It therefore makes sense to apply a Gaussian window in the time domain

$$G(t)=C(t)\exp(-\gamma t^2), \tag{24}$$

so that

$$\hat{G}(\omega)=\int_{-\infty}^{\infty}dte^{i\omega t}G(t)$$

$$=\sqrt{\frac{\pi}{\gamma}}\int_{-\infty}^{\infty}dw'\hat{C}(\omega-\omega')e^{-\omega'^2/(4\gamma)} \tag{25}$$

for large ω (i.e., if the asymptotic form (23) holds for the frequency $\omega-2\gamma^{1/2}$), and Eq. (25) can be evaluated in the form

$$\hat{G}(\omega)=\sqrt{\frac{\pi}{\gamma}}A\int_{-\infty}^{\infty}dw'e^{-(\omega-\omega')/\omega_0}e^{-\omega'^2/(4\gamma)}$$

$$=2\pi Ae^{\gamma/\omega_0^2}e^{-\omega/\omega_0}. \tag{26}$$

Thus plotting $[\ln\hat{G}(\omega)]$ vs ω we can obtain α from the slope and A from the intercept. It should be noted that while we have found this method to be quite useful for obtaining high-frequency information from the correlation function, in most situations this procedure was not used, since using the Fourier transform of $F(t)$ itself within the Wiener–Khinchin theorem was found to work better.

IV. EFFECT OF PHYSICAL PARAMETERS

Typical results for the vibrational relaxation rates were shown (Figs. 2 and 3) and discussed above. It was established that in the high-frequency regime, well above the solvent cutoff frequency, the vibrational relaxation rate associated with an isolated molecular mode (e.g., a diatomic impurity molecule) can be represented by an exponential function of the mode frequency:

$$k_{VR}=Ae^{-\omega/\omega_0}. \tag{27}$$

Table I gives fitted values for the parameters A and ω_0 obtained for the ''standard'' system defined in Sec. II and for its Lennard-Jones counterpart, as well as for variations of these systems. These variations are derived from the standard system by changing the solvent molecular mass, its moment of inertia, and the rotational characteristics of the solute molecule: In some of the simulations the solute is not allowed to rotate, making it possible to examine the role played by the corresponding local libration in the relaxation process. In all cases, the fit to the form (27) is based on the results obtained in a finite frequency range, typically 500–1300 cm^{-1} for the case of a polar solvent.[30]

TABLE I. Parameters for the vibrational relaxation rate, Eq. (27), for several model systems: The ''standard'' and the corresponding LJ systems, the related systems with restricted solute rotational motion, and systems related to the ''standard'' systems with different solvent mass or moment of inertia.

System	A (ps^{-1})	ω_0 (cm^{-1})
''standard''	26.4	112.5
LJ	26.7	103.3
''standard''-nonrotating solute	36.3	91.2
LJ-nonrotating solute	20.6	82.9
''standard''; $m\times10$	73.2	88.6
''standard''; $I\times10$	36.3	94.2
''standard''; $I\times100$	40.2	104.6

It is seen that both A and ω_0 depend on the solvent and impurity parameters. The effect on ω_0 is more significant because it appears exponentially in the rate expression. In particular, the importance of the local librational mode is seen by comparing the values of ω_0 for rotating and nonrotating solute. The effect of solvent rotational motion, inferred from comparing results obtained for different moments of inertia I, is relatively small for the present model system. Note that Fig. 1 similarly shows a relatively weak effect of the molecular rotations on the translational spectrum.[31]

V. QUANTUM EFFECTS: THE CO–Ar SYSTEM

Figures 5 and 6 show our results for the classical vibrational relaxation rate [based on Eqs. (1) and (2)] for the Ar–CO system (see Sec. II for details of the model system). Figure 5 displays $k_{VR}(\omega)$ as a function of mode frequency ω, at three temperatures: 20, 150, and 300 K, while Fig. 6 compares, at 20 K, the vibrational relaxation rate computed using a model which allows rotational/librational motion of the CO impurity and the rate obtained from a model which forbids this motion. Note that the full lines in Figs. 5 and 6 are identical. Based on our discussion above we can assert that k_{VR} is of the form (27). A fit to this form yields the results in Table II: For the CO frequency, $\omega\cong2140\ cm^{-1}$ in the matrix; using these parameters in Eq. (27) yields k_{VR} (classical simulation)$=2.14\cdot10^{-20}\ s^{-1}$ at $T=20$ K. This unphysically low result must be multiplied by the quantum correction factor Q [cf. Eqs. (1)–(5)],

$$Q=\frac{\tanh(\beta\hbar\omega/2)}{\beta\hbar\omega/2}\frac{\int_0^{\infty}dt\ \cos(\omega t)\langle[F(t),F(0)]_+\rangle_{QM}}{\int_{-\infty}^{\infty}dt\ \cos(\omega t)\langle F(0)F(t)\rangle_C}. \tag{28}$$

We recall[7] that $Q=1$ for a system characterized by a linear coupling between a harmonic bath and a harmonic impurity;

Downloaded 21 Mar 2004 to 132.66.16.12. Redistribution subject to AIP license or copyright, see http://jcp.aip.org/jcp/copyright.jsp

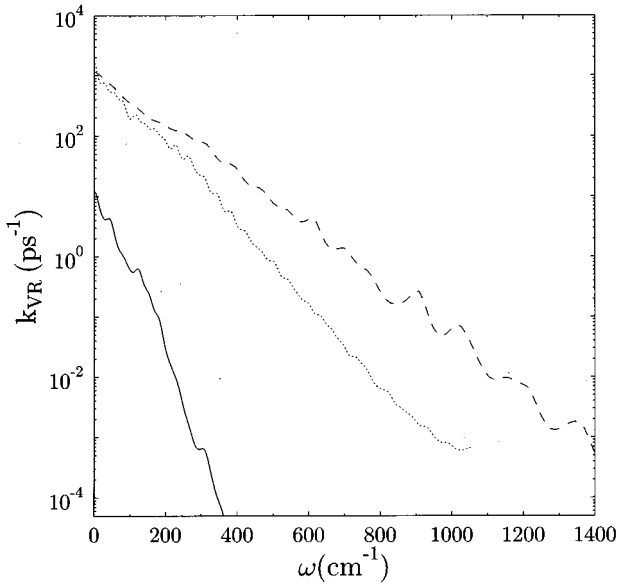

FIG. 5. The *classical* vibrational relaxation rate [Eqs. (1) and (2)] as a function of impurity frequency for a system characterized by the interaction parameters of a CO molecule embedded in an Ar matrix at $T=20$ (full line), 150 (dotted line), and 300 K (dashed line).

however, this is no longer the case for processes dominated by multiphonon transitions. In general, Q cannot be calculated exactly, and several ways to approximate it were suggested.[32–35] Here we use an approximate expression derived by Nitzan and Jortner[36,37] for a model which assumes a simple nonlinear coupling between a harmonic impurity of frequency ω and a harmonic bath:

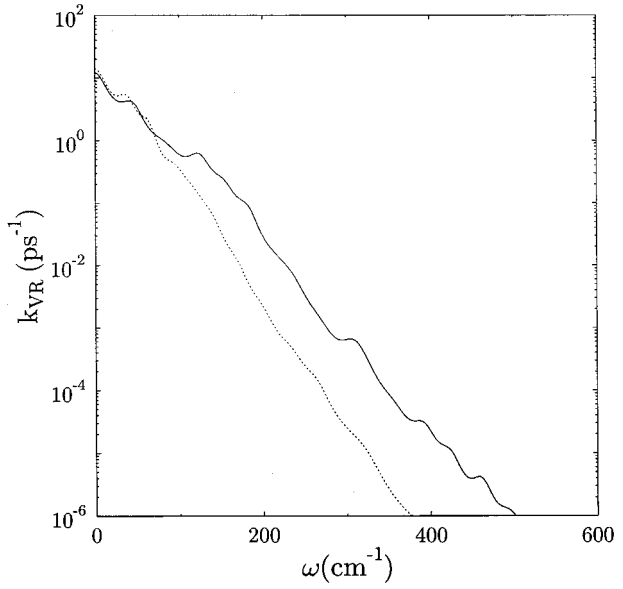

FIG. 6. The full line is identical to the corresponding line of Fig. 5. The dotted line represents the vibrational relaxation rate computed for the same system under the restriction that the CO molecule is not allowed to rotate.

TABLE II. Parameters for vibrational relaxation rate, Eq. (27), for the Ar–CO system.

System	A (ps^{-1})	ω_0 (cm^{-1})
20 K	33.4	28
20 K (nonrotating CO)	28.8	22
150 K	1550.	65
300 K	880.	103

$$Q \cong \frac{e^{\beta\hbar N\omega_D}-1}{(e^{\beta\hbar\omega_D}-1)^N}\,\frac{(\beta\hbar\omega_D)^N}{\beta\hbar N\omega_D}, \tag{29}$$

where ω_D is the ''Debye frequency'' of the bath and $N=\omega/\omega_D$ is the order of the dominant multiphonon process. It should be emphasized that ω_D appearing in this expression represents the highest frequency bath mode coupled to the impurity, irrespective of the validity of the Debye model for the environment.

For solid argon, $\omega_D \cong 64$ cm^{-1}, hence $N \cong 33.4$. Using these numbers in (29) yields $Q \cong 1.2\cdot 10^{20}$ and $k_{VR} \cong 2.5$ s^{-1}, which is compared favorably to the upper bound for this rate estimated from experimental results.[38] It should be emphasized that the theoretical result may be too high: The $\omega_D=64$ cm^{-1}corresponds to the pure solid argon and disregards the higher frequency local modes associated with the CO impurity. Such modes arise both because the mass of CO is smaller than that of Ar and because of the libration of the CO molecule in the solvent cage. We may estimate the effect of the librational motion from the data displayed in Fig. 6. Assuming that for the nonrotating CO case $\omega_D=64$ cm^{-1}, and that the rate is proportional to $\exp(-\alpha\cdot\omega/\omega_D)$ [so that ω_0 in Eq. (27) is ω_D/α], with the same α in the rotating and nonrotating CO cases, yields for the rotating CO system (using numbers from Table II) $\omega_D \cong 64\cdot 28/22 = 82$ cm^{-1} and correspondingly, $N \cong 26.1$. With these parameters, Eq. (29) yields $Q=1\cdot 10^{18}$ and $k_{VR} \cong 0.021$ s^{-1}.

While the absolute values given by the above estimates should not be taken too seriously, the trends observed suggest that we have indeed identified the main physical factors affecting vibrational relaxation in such systems. In particular, the magnitude of the quantum correction factor emphasizes the need to include it in any computation of the relaxation rate. The large sensitivity to the local mode structure associated with the impurity motion in the solvent cage makes it clear that any estimate of the relaxation rate should take this input into consideration. These observations suggest that a direct numerical computation of the quantum correction factor, Eq. (28), is needed in any simulation approach to the vibrational relaxation of high-frequency modes.

VI. CONCLUSIONS

Numerical computation of vibrational energy relaxation rates of high-frequency modes in condensed phases is facilitated by using appropriate time correlation functions derived from linear response theory. Two sources of difficulty remain: (a) The numerical problem posed by the need to evalu-

Downloaded 21 Mar 2004 to 132.66.16.12. Redistribution subject to AIP license or copyright, see http://jcp.aip.org/jcp/copyright.jsp

ate high-frequency Fourier transforms of the computed time correlation functions, and (b) the uncertainty involving the relation between the computed classical and the needed quantum correlation function. In this paper we have shown that evaluating the needed Fourier transform, a very weak signal in the presence of much stronger irrelevant ones, can be done in a satisfactory way using available methods from the signal processing literature. The need for great accuracy in this calculation is relaxed considerably using the observation that the resulting signal, and correspondingly the rate, depends exponentially on the frequency. We have also analyzed the quantum correction factor using an approximate expression derived for harmonic solid environments. The quantum correction factor can change the rate by many orders of magnitude for high-frequency modes at low temperatures, and its numerical value depends sensitively on system parameters, in particular the relaxing frequency and the solvent cutoff frequency. Analysis of the computational results also underline the importance of local modes associated with the relaxing impurity molecule, e.g., its center of mass motion and its librational motion in the solvent cage.

ACKNOWLEDGMENT

This research is supported in part by the Israel Science Foundation. We thank Mark Ratner for very helpful discussions. P. Graf is thankful to the Minerva-Stiftung for a post doctoral fellowship.

APPENDIX: ASYMPTOTIC EXPANSION OF EQ. (7)

In this Appendix we evaluate the asymptotic form of the Fourier transform

$$J(\omega)=2\int_0^\infty dt\ \cos(\omega t)C(t) \tag{A1}$$

of the Kubo function

$$C(t)=\exp\left[-\alpha^2\left(\frac{t}{\alpha}-1+e^{-t/\alpha}\right)\right]. \tag{A2}$$

[Note that the functions $\phi(t)$and $I(\omega)$ defined in Chapter 2.1 of Ref. 16 correspond to $C(t\Delta)$ and $(1/(2\pi\Delta))J(\omega/\Delta)$, where ω is measured from the line center.] The parameter α and the time t determine the behavior of the Kubo function as follows: For $t/\alpha\to 0$, $C(t)=\exp(-t^2/2)$, while in the opposite limit, $t/\alpha\to\infty$, $C(t)=\exp(-\alpha t)$. Consequently, it is a common belief that $J(\omega)$ behaves as a Lorentzian, $(\omega^2+\alpha^2)^{-1}$, near the absorption center, and as a Gaussian, $\exp(-\omega^2/2)$, in the band edges. However, while a Gaussian behavior in the band edges may indeed be expected on physical grounds, it is *not* the result of Eqs. (6) and (7). The asymptotic $\omega\to\infty$ form of $J(\omega)$ can be obtained by following the procedure described in Ref. 40, Chapter 2.8: An integral of the form $\int_\alpha^\beta e^{i\omega t}\phi(t)dt$ with $\phi(t)$ N times continuously differentiable in the interval $\alpha\leqslant t\leqslant\beta$ can be represented by

$$\int_\alpha^\beta e^{i\omega t}\phi(t)dt=B_N(t)-A_N(t)+\mathcal{O}(\omega^{-N}), \tag{A3}$$

where

$$A_N(\omega)=\sum_{n=0}^{N-1} i^{n-1}\phi^{(n)}(\alpha)\omega^{-n-1}e^{i\omega\alpha}, \tag{A4}$$

$$B_N(\omega)=\sum_{n=0}^{N-1} i^{n-1}\phi^{(n)}(\beta)\omega^{-n-1}e^{i\omega\beta},$$

and where $\phi^{(n)}=d^n\phi/dt^n$. Equation (A3) holds also when $\alpha\to\infty$ or $\beta\to\infty$, provided that $\phi^{(n)}(t)\to 0$ for $t\to\pm\infty$ for $n=0,1,...,N-1$ and that $\phi^{(N)}(t)$ is integrable in (α,β). Using these results in Eq. (7) leads to the asymptotic expansion

$$J(\omega)\sim 2\sum_{m=1}^{\infty}(-1)^m C^{(2m-1)}(0)\omega^{-2m};\quad \omega\to\infty. \tag{A5}$$

For the Kubo function, Eq. (6), we find $C^{(2m-1)}(0)=0$ for $m=1$and $C^{(2m-1)}(0)=1/\alpha$ for $m=2$, and thus $J(\omega)\sim\omega^{-4}$ as $\omega\to\infty$. For large α, we have found that a good approximation for $J(\omega)$ is given by the ansatz

$$J(\omega)\cong\sqrt{2\pi e}^{-(\omega^2/2)}+\frac{2}{\alpha}\omega^{-4}, \tag{A6}$$

which corresponds to a transition from a Gaussian behavior at small ω to the asymptotic ω^{-4} dependence at large ω, at a cross-over frequency ω_c given as the solution of

$$\omega_c=\sqrt{2\ln\left(\left(\frac{\pi}{2}\right)^{1/2}\alpha\right)+8\ln\ \omega_c}. \tag{A7}$$

[1] B. J. Berne, M. E. Tuckerman, J. E. Straub *et al.*, J. Chem. Phys. **93**, 5084 (1990).
[2] M. Tuckerman and B. J. Berne, J. Chem. Phys. **98**, 7301 (1993).
[3] R. M. Whitnell, K. R. Wilson, and J. T. Hynes, J. Phys. Chem. **94**, 8625 (1990).
[4] R. M. Whitnell, K. R. Wilson, and J. T. Hynes, J. Chem. Phys. **96**, 5354 (1992).
[5] M. Bruehl and J. T. Hynes, Chem. Phys. **175**, 205 (1993).
[6] S. A. Adelman, R. Muralidhar, and R. H. Stote, J. Chem. Phys. **95**, 2738 (1991).
[7] J. S. Bader and B. J. Berne, J. Chem. Phys. **100**, 8359 (1994).
[8] I. Benjamin and R. M. Whitnell, Chem. Phys. Lett. **204**, 45 (1993).
[9] S. A. Egorov and J. L. Skinner, J. Chem. Phys. **105**, 7047 (1996).
[10] R. Rey and J. T. Hynes, J. Chem. Phys. **104**, 45 (1996).
[11] F. E. Figueirido and R. M. Levy, J. Chem. Phys. **97**, 703 (1992).
[12] S. Gnanakaran and R. M. Hochstrasser, J. Chem. Phys. **105**, 3486 (1996).
[13] F. Legay, in *Chemical and Biochemical Applications of Lasers* (Academic, New York, 1977), Vol. II, p. 43.
[14] G. Goodyear and R. M. Stratt, J. Chem. Phys. **105**, 10050 (1996).
[15] A. Nitzan, S. Mukamel, and J. Jortner, J. Chem. Phys. **63**, 200 (1975).
[16] R. Kubo, M. Toda, and N. Hashitsume, *Statistical Physics II* (Springer-Verlag, Berlin, 1985).
[17] The explicit statement made in Ref. 16 is as follows: ''By general property of a Fourier transform, the behavior of $J(\omega)$ in the neighborhood of $\omega=0$ is governed by the asymptotic behavior of $C(t)$ for large t, and that for large ω by that of $C(t)$for small t. Accordingly, the shape of the spectrum at the center to a Lorentzian form which corresponds to the long-time approximation. However the wings are close to a Gaussian form, corresponding to the short-time approximation.''
[18] W. L. Jorgensen, J. Chandrasekhar, and J. D. Madura, J. Chem. Phys. **79**, 926 (1983).
[19] J. Zhu and R. I. Cukier, J. Chem. Phys. **99**, 5384 (1993).
[20] H. Gordon and S. Goldman. Mol. Simul. **2**, 177 (1989).
[21] P. H. Berens and K. R. Wilson, J. Chem. Phys. **74**, 4872 (1981).
[22] H. E. Hallam, *Vibrational Spectroscopy of Trapped Species* (Wiley, New York, 1973).

Downloaded 21 Mar 2004 to 132.66.16.12. Redistribution subject to AIP license or copyright, see http://jcp.aip.org/jcp/copyright.jsp

[23] E. Neria and A. Nitzan, J. Chem. Phys. **96**, 5433 (1992).
[24] S. W. de Leeuw, J. W. Perram, and E. R. Smith, Proc. R. Soc. London, Ser. A **373**, 27 (1980).
[25] J. W. Perram, H. G. Petersen, and S. W. de Leeuw, Mol. Phys. **65**, 875 (1988).
[26] C. W. Therrien, *Discrete Random Signals and Statistical Signal Processing* (Prentice Hall, Englewood Cliffs, NJ, 1992).
[27] W. H. Press, B. P. Flannery, S. A. Teukolsky *et al.*, *Numerical Recipes* (Cambridge University Press, Cambridge, 1986).
[28] F. J. Harris, Proc. IEEE **66**, 51 (1978).
[29] M. Cho, J. Chem. Phys. **105**, 10 755 (1996).
[30] These numerical results were obtained relatively early in our study, and are based on simulations with reaction field boundary conditions which, as seen in Fig. 2, give reliable results only at a relatively narrow frequency range.
[31] This property of the Stockmayer model understandably deviates from the behavior of many ''real'' liquids with similar partial atomic charges, where librational modes appear at higher frequencies.
[32] P. Schofield, Phys. Rev. Lett. **4**, 39 (1960).
[33] P. A. Egelstaff, Adv. Phys. **11**, 203 (1962).
[34] L. Frommhold, *Collision-Induced Absorption in Gases* (Cambridge University Press, Cambridge, 1993).
[35] S. A. Egorov and B. J. Berne, J. Chem. Phys. **107**, 6050 (1997).
[36] A. Nitzan and J. Jortner, Mol. Phys. **25**, 713 (1973).
[37] A. Nitzan, S. Mukamel, and J. Jortner, J. Chem. Phys. **60**, 3929 (1974).
[38] The dominant relaxation in pure Ar/CO samples is via the radiative channel—IR fluorescence by the vibrationally excited CO (Ref. 39), and the upper bound is estimated (Ref. 13) in correspondence with this observation.
[39] H. Dubost and R. Charneau, Chem. Phys. **12**, 407 (1976).
[40] A. Erdelyi, *Asymptotic Expansions* (Dover, London, 1956).

Downloaded 21 Mar 2004 to 132.66.16.12. Redistribution subject to AIP license or copyright, see http://jcp.aip.org/jcp/copyright.jsp